Developing inhibitors of the p47phox-p22phox protein-protein interaction by fragment-based drug discovery

Journal:	*Journal of the American Chemical Society*
Manuscript ID	ja-2019-04205r
Manuscript Type:	Article
Date Submitted by the Author:	18-Apr-2019
Complete List of Authors:	Bach, Anders; University of Copenhagen, Department of Drug Design and Pharmacology Solbak, Sara; University of Copenhagen, Department of Drug Design and Pharmacology Zang, Jie; University of Copenhagen, Department of Drug Design and Pharmacology Narayanan, Dilip; University of Copenhagen, Department of Drug Design and Pharmacology Høj, Lars; University of Copenhagen, Department of Drug Design and Pharmacology Bucciarelli, Saskia; University of Copenhagen, Department of Drug Design and Pharmacology Softley, Charlotte; Helmholtz Zentrum München Institut für Strukturbiologie; Technical University of Munich, Department of Chemistry Meier, Sebastian; Technical University of Denmark, Department of Chemistry Langkilde, Annette; University of Copenhagen, Department of Drug Design and Pharmacology Gotfredsen, Charlotte; Danmarks Tekniske Universitet, Department of Chemistry Sattler, Michael; Technische Universität München, Chemistry

Developing inhibitors of the p47phox-p22phox protein-protein interaction by fragment-based drug discovery

Sara Marie Øie Solbak[1], Jie Zang[1], Dilip Narayanan[1], Lars Jakobsen Høj[1], Saskia Bucciarelli[1], Charlotte Softley[2,3], Sebastian Meier[4], Annette Eva Langkilde[1], Charlotte Held Gotfredsen[4], Michael Sattler[2,3], Anders Bach[1]

[1]Department of Drug Design and Pharmacology, Faculty of Health and Medical Sciences, University of Copenhagen, Universitetsparken 2, 2100 Copenhagen, Denmark

[2]Institute of Structural Biology, Helmholtz Zentrum München, 85764 Neuherberg, Germany

[3]Biomolecular NMR and Center for Integrated Protein Science Munich at Department of Chemistry, Technical University of Munich, 85747 Garching, Germany.

[4]Department of Chemistry, Technical University of Denmark, Kemitorvet, 2800 Kgs Lyngby, Denmark

Correspondence: anders.bach@sund.ku.dk

Running title: Targeting p47phox by fragment-based drug discovery

Keywords: NADPH oxidase, NOX2, p47phox, fragment-based drug discovery, protein-protein interaction inhibitors, dimeric ligands

Author e-mails: S.M.Ø.S. (sara.solbak@sund.ku.dk); J.Z. (jie.zang@sund.ku.dk); D.N. (dilip.narayanan@sund.ku.dk); L.J.H (lars.j.hoej@gmail.com); S.B. (saskia.bucciarelli@sund.ku.dk); C.S. (charlotte.softley@helmholtz-muenchen.de); S.M. (semei@kemi.dtu.dk); A.E.L. (annette.langkilde@sund.ku.dk); C.H.G. (chg@kemi.dtu.dk); M.S. (sattler@helmholtz-muenchen.de); A.B. (anders.bach@sund.ku.dk)

Graphical abstract

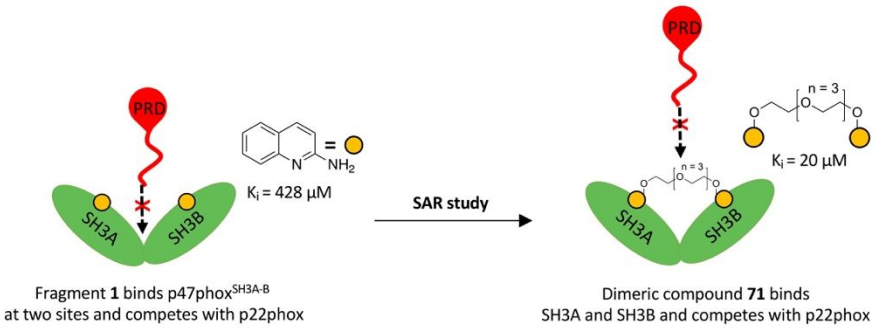

Abstract

NADPH oxidase isoform 2 (NOX2) is an enzyme complex, which generates reactive oxygen species (ROS). Excessive ROS contributes to oxidative stress, involved in inflammation, cancer and CNS diseases. A way of attenuating oxidative stress is to prevent triggering of NOX2. Upon activation, the p47phox-p67phox-p40phox subunits relocate from the cytosol to the plasma membrane where they associate with flavocytochrome b558 and form active NOX2. The p47phox-p22phox interaction is critical for this complex, and p47phox has thus been suggested as target for therapeutic intervention. Here, we identify several small-molecule fragments to be used as starting points for developing inhibitors of the p47phox-p22phox interaction. We screened a library of 2,500 fragments for binding to the tandem SH3 domain SH3A-B of p47phox (p47phox^{SH3A-B}). We used fluorescence polarization and a thermal shift assay for screening, and validated the hits by surface plasmon resonance including an inhibition assay, providing information on the binding site at p47phox^{SH3A-B}. Based on the validation, eight hits with equilibrium dissociation constant between 400–600 μM were selected for structural studies. These revealed two small-molecule binding pockets in the elongated conformation of p47phox^{SH3A-B}. Interestingly, two fragment hits (**1** and **2**) bound to both of these binding sites and competed with p22phox for binding to p47phox^{SH3A-B}. Sixty-five analogs were generated and tested in a structure activity relationship study, leading to a dimeric compound with low μM affinity (K_i of 20 μM) towards p47phox^{SH3A-B}. To our knowledge, this is the first report of druglike molecules able to bind p47phox and inhibit its interaction with p22phox.

Introduction

NADPH oxidase isoform 2 (NOX2) is a multi-protein enzyme complex that is highly expressed in phagocytes and which catalyzes the reduction of molecular oxygen to superoxide anion ($O2^{\bullet-}$). This reactive oxygen species (ROS) generating enzyme is known to have a key role in innate immunity, as demonstrated in chronic granulomatous disease (CGD) caused by an inherited deficiency of NOX2, where the phagocytes fail to kill invading microorganisms [1]. Excessive ROS production by NOX2 on the other hand contributes to oxidative stress and is connected to a wide range of diseases involving inflammation, diabetes, and cancer [2-4]. Furthermore, NOX2 via ROS production within the central nervous system (CNS), contributes to brain damage resulting from traumatic brain injury, reperfusion injury in stroke, and to the pathologies of neurodegenerative diseases [1, 4-7].

The inactive form of NOX2 consists of a membrane-bound flavocytochrome b558, a heterodimer of gp91phox (NOX2) and p22phox, three cytosolic proteins, p40phox, p47phox and p67phox, and a small G protein Rac GTPase, which form a complex in the cytosol [4, 8]. NOX2 in phagocytic cells is activated by Ca^{2+}-influx activating the phosphokinase C (PKC), which further phosphorylates C-terminal serine residues located in the autoinhibitory region (AIR) and the proline-rich region (PRR), leading to activation of p47phox [9-12]. The phosphorylation causes a conformational change of p47phox, allowing the cytosolic proteins to relocate to the plasma membrane where they associate with flavocytochrome b558, forming the active NOX2 complex. In its inactive state, the p47phox tandem Src Homology 3 (SH3) domain (SH3A-B) is occupied by the AIR of p47phox. However, upon p47phox phosphorylation in the AIR domain, the conformational change involves detachment of the AIR domain from the SH3A-B domain, allowing SH3A-B to bind to the proline-rich domain (PRD) of p22phox instead [13, 14]. The truncated p47phox SH3A-B ($p47phox^{151–286}$) without the AIR (here referred to as $p47phox^{SH3A-B}$) is considered a model protein of activated p47phox, as it has an open tandem SH3 domain and does not require phosphorylation to bind to p22phox [13, 15]. The structure of the tandem SH3 domain including the AIR ($p47phox^{151-342}$; here referred to as $p47phox^{AIR}$) and $p47phox^{SH3A-B}$ in complex with the p22phox derived peptide $p22phox^{149-168}$ have previously been investigated by X-ray crystallography, NMR, and small angle X-ray scattering (SAXS) [13, 15-18]. By X-ray crystallography, both $p47phox^{AIR}$ and $p47phox^{SH3A-B}$ in complex with $p22phox^{149-168}$ were found to form intertwined dimers [13, 18]. However, by NMR and SAXS analysis, under physiologically more relevant conditions in solution, the proteins were found to be monomeric [15, 16]. Interestingly, the SAXS studies revealed an overall more compact conformation of the $p47phox^{SH3A-B}$-p22phox complex than for the more extended apo $p47phox^{SH3A-B}$. Furthermore, the binding interface of $p47phox^{SH3A-B}$ to $p22phox^{149-168}$ was characterized by NMR chemical shift perturbation (CSP) analysis based on ^{1}H-^{15}N HSQC NMR titration experiments. In particular, for the three tryptophan residues in SH3A (Trp^{193}, Trp^{194} and Trp^{204}) and the two in SH3B (Trp^{263} and Trp^{264}), significant CSPs were observed during titration with $p22phox^{149-168}$ [15]. This finding reflects that $p22phox^{149-168}$ stably interacts with a region composed by both SH3 domains forming a crevice in the middle of the tandem SH3 domain, as shown by NMR structure determination (PDB ID: 1WLP) [15].

The binding between p47phox and p22phox is essential for NOX2 activation, and p47phox has thus been suggested as a target for therapeutic intervention [5, 19]. However, the only small molecular compound reported to prevent NADPH oxidase activity by direct inhibition of the p47phox-p22phox interaction is ebselen (2-phenyl-1,2-benzisoselenazol-3(2H)-one) [19]. This is a synthetic seleno-organic ROS scavenging compound known to induce

cysteine-targeted oxidation followed by S-thiolation - an oxidative, reversible modification of the cysteine residues of proteins [20, 21]. In addition, it has been suggested that some apocynin derivates with antioxidant activity bind to p47phox [22, 23], but this was based on *in silico* studies only and no experimental evidence.

In this study, we initially investigated the mechanism of action of ebselen and found that it does not compete reversibly with p22phox for the p47phox^{SH3A-B} binding pocket, but instead binds p47phox^{SH3A-B} covalently, leading to destabilization and aggregation of the protein. To find novel reversible inhibitors able to selectively inhibit the p47phox-p22phox interaction, we used a fragment-based drug discovery (FBDD) approach and screened a library of 2,500 fragments for binding to p47phox^{SH3A-B} by fluorescence polarization (FP) competition and thermal shift assay (TSA). Using SPR binding and competition assays, in addition to structural characterizations of the binding of these fragments to p47phox^{SH3A-B} by NMR CSP analysis and SAXS, we identified two potential fragments which can serve as scaffolds for developing new inhibitors of the p47phox-p22phox protein-protein interaction. Structure activity relationship (SAR) studies resulted in several compounds with enhanced affinity to p47phox^{SH3A-B}, the best ones being dimeric compounds which display a 13–30-fold higher affinity relative to the parent fragment hits.

Results

Assay development and validation by binding studies of p22phox to p47phox. In order to discover small molecular inhibitors of the p47phox-p22phox interaction, we developed an FP inhibition assay, a TSA and an SPR binding assay, which we validated by p22phox binding studies to p47phox. In the FP assay, the interaction of either a TAMRA labeled p22phox derived peptide p22phox$^{151-162}$ or a Cy5 labeled peptide p22phox$^{149-162}$ was measured with purified p47phox^{SH3A-B}. At constant TAMRA or Cy5 probe concentrations, increasing amounts of p47phox^{SH3A-B} gave saturable increases in polarization with equilibrium dissociation constants (K_D) of 4.0 ± 0.3 μM and 0.88 ± 0.02 μM, respectively (Fig. S1A-B). As positive controls, we tested whether the two peptides p22phox$^{151-162}$ and p22phox$^{149-168}$, derived from the PRD of p22phox, could dissociate the labeled peptides. The polarization was decreased for both p22phox$^{151-162}$ and p22phox$^{149-168}$ with inhibitory constants (K_i) of ~8 μM and 0.3 μM, respectively (Fig. S1C-D). The affinity values correspond to previous literature and the reporting of a >10-fold increase in affinity for p47phox binding to p22phox$^{149-168}$ (or longer peptides), compared to the shorter p22phox$^{151-162}$ [13, 15, 19].

In the TSA, the melting point (T_m) of p47phox^{SH3A-B} was increased by p22phox$^{151-162}$ and p22phox$^{149-168}$ with a ΔT_m of 4.0 °C and 9.2 °C over a concentration range of 0–200 μM and 0–100 μM, respectively (Fig. S2). This increase correlates well with the FP results, showing a stronger binding affinity of p22phox$^{149-168}$ to p47phox^{SH3A-B} compared to p22phox$^{151-162}$.

For the SPR assay, p47phox^{SH3A-B} was covalently immobilized to a biosensor chip and activity of the immobilized protein was validated by injections of p22phox$^{151-162}$, p22phox$^{149-168}$ and p22phox$^{149-162}$, all containing the PRD of p22phox, known to bind to p47phox^{SH3A-B}. Binding of p22phox$^{151-162}$, p22phox$^{149-162}$ and p22phox$^{149-168}$ to p47phox^{SH3A-B} gave affinities (K_D) of 15, 3.8 and 0.34 μM, respectively (Fig. S3A-C Table S1), consistent with the FP affinities above (Fig. S1) and from previous reports [13, 15]. The AIR domain of p47phox was suggested to prevent p47phox from interacting with p22phox by binding to the tandem SH3 domain of p47phox when in the inactive state, as shown by lack of binding between p47phox full-length or p47phox^{AIR} with peptides containing the PRD of p22phox [13, 24]. Accordingly, injecting p22phox$^{151-162}$ and p22phox$^{149-168}$ over immobilized p47phox^{AIR} (Fig. S3D-E) gave affinities 77

times lower (K_D = 1.2 mM) for p22phox$^{151-162}$ and 19 times lower (K_D = 6.6 μM) for p22phox$^{149-168}$ than when binding to p47phox^{SH3A-B} (Fig. S3D-E and Table S1).

Interaction between p47phox and ebselen. Ebselen is described in literature as preventing NOX2 activation by inhibiting the direct interaction between p47phox and p22phox [19]. We therefore thought this compound could serve as a useful reference for the assays and investigated the mechanism of action in more detail. In FP, ebselen in the absence of the reducing agent tris-(2-carboxyethyl)phosphine (TCEP) yielded a K_i of 63 ± 6 μM, while a >10-fold increase in K_i (>300 μM) was observed with TCEP present in the buffer, which indicate a covalent binding mode. When prolonging the incubation time from 10 minutes to 2 hours in the FP assay without TCEP, the K_i was reduced to 12 ± 0.07 μM (Fig. 1A). To explore the interaction further, direct binding between ebselen and p47phox^{SH3A-B} was measured by SPR. Ebselen strongly bound p47phox^{SH3A-B}, with an almost non-reversible binding kinetic (slow dissociation rate) (Fig. 1B). The binding was however reversed by the TCEP (Fig. 1B and Fig. S4A). Furthermore, LCMS analysis of p47phox^{SH3A-B} with ebselen showed a total mass of 17573.1 Da (Fig. 1C), which compared to the mass of p47phox^{SH3A-B} without ebselen (17299.5 Da) (Fig. S4B) corresponds to a mass-increase similar to the molecular weight of ebselen (274.2 Da). This result demonstrates that ebselen forms a stable complex with p47phox^{SH3A-B}. This together with the results from FP and SPR showing lack of binding of ebselen to p47phox^{SH3A-B} in the presence TCEP (which reduces cysteine residues and prevents them from forming disulfide-bonds), demonstrates a covalent interaction of ebselen with the only cysteine (Cys^{196}) of p47phox^{SH3A-B} (Fig. 1D-E).

To investigate structural alterations of p47phox^{SH3A-B} when binding to ebselen, we performed SAXS studies. The SAXS data indicated aggregation of p47phox^{SH3A-B} in the presence of ebselen, evident by a strong increase in the maximum dimension of the particles (D_{max}) (starting at 235 Å, compared to the 86 Å without ebselen). The corresponding SAXS-derived radius of gyration (R_g=67.6 Å) and the concentration-normalized scattering intensity at q=0 (I(0)/c =17.2 a.u) were also higher than without ebselen (26.5 Å and 1.1 a.u, respectively) (Fig. 1F-G, Table S2). The aggregation was observed shortly after sample preparation and increased over time (data not shown).

Overall, ebselen was found to covalently bind to Cys^{196} of p47phox^{SH3A-B}, leading to destabilization and aggregation. Thus, ebselen inhibits NOX2 by destabilizing p47phox^{SH3A-B} rather than by occupying the p22phox binding pocket. We found this mechanism of action unsuitable for further investigations of inhibitors of the p47phox-p22phox interaction, and instead used the p22phox peptides p22phox$^{151-162}$ and p22phox$^{149-168}$ as controls for screening and validation assays.

Fragment screening and hit validation. To develop direct inhibitors of the p47phox-p22phox interaction, 2,500 rule of 3 compliant fragments [25] were screened at 1 mM for binding to p47phox^{SH3A-B} in the FP assay, using the Cy5 probe, and at 0.5 mM for inducing thermal stabilization of p47phox^{SH3A-B} by TSA. The FP screening resulted in 75 fragments (3.0% hit rate) that caused at least a 20% decrease in polarization relative to the DMSO control. The TSA screen resulted in 109 fragment hits (4.4% hit rate), where a hit was defined as a fragment that induced a ΔT_m > 0.9°C relative to the negative control, and a sigmoidal melting curve with a fluorescence window in the proximity of the controls.

The 75 hits from the primary FP screen were validated in a 6-point FP dose-response experiment (63 μM – 2 mM) in the absence and presence of 0.01% Triton-X to exclude aggregation-based promiscuous inhibitors [26-28]. The fragments were also tested using the TAMRA-probe, in the absence of p47phox^{SH3A-B}, and by assessing the stability of the total fluorescence intensity (FLINT), in order to remove false-positives due to fluorescence inner-filter effects [29-

33]. A total of 22 fragments had positive results in at least 3 of 4 tests and were selected as validated FP hits (0.9% hit rate) (the FP validation data for **1** are shown in Fig. 2A). The hits from the primary TSA screen were validated in a 4-point TSA dose-response experiment (0.25-2 mM). A total of 98 fragments (3.9% hit rate) showed a dose-dependent increment in ΔT_m, and were thus considered validated TSA hits (the TSA data for **1** are shown in Fig. 2B). Only 3 hits were validated in both FP and TSA.

Twenty-four of the validated fragments contained potentially reactive groups, such as thiourea and nitriles, or had structural similarity to ebselen. We therefore tested these fragments in LCMS to see if they would bind covalently to p47phox^{SH3A-B}, in analogy to ebselen (Fig. 1C). One fragment, (2-(3-(trifluoromethyl)phenyl)isothiazol-3(2H)-one) showed a mass increase equal the molecular weight of the fragment (245.2 Da), indicating a similar binding mechanism as for ebselen, and was removed from further studies, leaving 116 fragment hits validated in FP or TSA (Fig. 2C).

Fragment hits validated for binding to p47phox^{SH3A-B} by SPR. The 116 validated hits were further assayed for direct binding to p47phox^{SH3A-B} by SPR in two-fold serial dilutions over immobilized p47phox^{SH3A-B}. Seventy-two fragments showed a concentration dependent response, thus confirming interaction with p47phox^{SH3A-B} (SPR data of **1** are shown in Fig. 2D), while 39 fragments displayed low or no binding and five fragments showed non-fragment like binding with slow on- or off-rates (see examples in Fig. 2E-F).

To evaluate whether the 72 SPR validated fragments bind to or interfere with the binding interface of p22phox at p47phox, we performed an SPR inhibition assay. The fragments (1 mM) were injected over immobilized p47phox^{SH3A-B}, where the binding interface between p47phox^{SH3A-B} and p22phox was blocked by p22phox$^{149-168}$ included at saturating concentration (10 μM) in the running and ligand buffer [34]. Following this assay, a similar injection was performed over the p47phox^{SH3A-B} surface not blocked by p22phox$^{149-168}$. A reduced binding of the fragments to p47phox^{SH3A-B} blocked by p22phox, would indicate that the fragments bind to the same interface at p47phox^{SH3A-B} as p22phox. Out of the 72 tested fragments, 14 showed a reduced binding response in the inhibition assay, with a calculated metric S $\geq$0.15, corresponding to a reduction in response level of ~25% (data for p22phox$^{151-162}$ and fragment **1** are shown in Fig. S5 and Fig. 2G-H, respectively). The 14 fragment hits were checked for structural similarities to known pan-assay interference compounds (PAINS) or aggregators using the filtering tool FAFdrugs4 (Free ADME-Tox Filtering Tool) [35] and Aggregator Advisor [36]. One fragment containing a thioketone was flagged as a potential covalent binder. The SPR binding experiments and inhibition assays of the remaining 13 hits were repeated in order to confirm these. Two of the fragments showed only little reduction in binding in the presence of blocking peptide and were excluded, resulting in 11 SPR validated hits (cf. Venn diagram in Fig. 2I). Out of these, three had very weak affinities to p47phox, and thus eight fragments (Fig. 2J) were selected for further investigations by NMR and SAXS. SPR sensorgrams and biophysical data for these are shown in Fig. S6 and Table 1.

NMR chemical shift changes in p47phox^{SH3A-B} upon binding to fragment hits. The SPR inhibition assay shows that p22phox prevents binding of the fragments, which indicates that our fragment hits bind to the same site of p47phox^{SH3A-B} as p22phox, and thus to the same compact conformation of p47phox^{SH3A-B}. To explore this further, we analyzed the CSPs in ^{1}H-^{15}N HSQC spectra focusing on the five Trp key residues considered in the binding interface of p47phox^{SH3A-B} to p22phox (Fig. 3A) [15]. As described in the literature, large chemical shift changes with slow exchange at the NMR chemical shift time scale were observed for all five well-resolved Trp indole NHs of p47phox^{SH3A-B} when titrated

with p22phox$^{149\text{-}168}$ (p47phox$^{SH3A\text{-}B}$:p22phox$^{149\text{-}168}$ ratios 1:0, 2:1, 1:1, 1:2 and 1:4) (Fig. 3B-C and S7). The assignment of the Trp indole signals of p47phox$^{SH3A\text{-}B}$ in complex with p22phox$^{149\text{-}168}$ was obtained from Ogura et al [15], and the tentative assignment of Trp indole signals of the free p47phox$^{SH3A\text{-}B}$ was derived from titration experiments with p22phox$^{149\text{-}168}$ (Fig. S7). Subsequently, titrations with all eight fragment hits were performed (p47phox$^{SH3A\text{-}B}$:fragment ratio 1:0, 1:5, 1:10 and 1:20) and the absolute CSP measured for the indole NH signals during titrations with each of the fragments were characterized (Fig. 3D, S8 and Table S3). All CSPs of the indole NHs of p47phox$^{SH3A\text{-}B}$ upon titration of p22phox$^{149\text{-}168}$ reflect binding in slow exchange. Fragment hits **1** and **2** were the only fragments showing CSPs for all five indole NHs of the Trps, including strong CSPs with slow to intermediate exchange binding kinetics for Trp residues Trp^{193}, Trp^{194} Trp^{204}, Trp^{263} and Trp^{264} situated both in the SH3A and SH3B region of p47phox$^{SH3A\text{-}B}$ (Table S3, Fig. S8A-B). Fragment hits **4**, **5** and **7** showed only weak CSP for one Trp indole NH (Trp^{193}) located in the SH3A domain, thus indicative of little influence on the magnetic environment of the indole NHs of p47phox$^{SH3A\text{-}B}$ upon binding to these fragments and binding to only the SH3A domain (Fig. S8G-I and M). Fragment hits **3**, **6** and **8** showed CSPs of three or four indole NHs, mostly characterized as weak.

Solution structure of p47phox$^{SH3A\text{-}B}$ upon fragment binding investigated by SAXS. The NMR CSP analysis with the eight fragment hits, showed CSPs to the Trp indole NHs in p47phox$^{SH3A\text{-}B}$, which are also affected by the binding of p22phox$^{149\text{-}168}$. This suggest that the fragments bound to the same compact conformation and binding site at p47phox$^{SH3A\text{-}B}$ as the p22phox-peptides. To confirm the results of Ogura et al. [15] and Yuzawa et al. [16] showing a more compact conformation of p47phox$^{SH3A\text{-}B}$ upon binding to p22phox, we performed SAXS studies of p47phox$^{SH3A\text{-}B}$ and the auto-inhibited form p47phox^{AIR} with and without the presence of the p22phox derived peptides. The pair-distance distribution functions of the SAXS data of p47phox$^{SH3A\text{-}B}$ when binding to p22phox$^{149\text{-}168}$ and p22phox$^{151\text{-}162}$ are narrower (Fig. 3E-F, Fig. S9A-B) and the Kratky plots more bell-shaped (Fig. S9C) than for the free p47phox$^{SH3A\text{-}B}$, thus indicating a more compact conformation of p47phox$^{SH3A\text{-}B}$ when binding to p22phox peptides and supporting the conclusions of Ogura et al. [15]. A similar compact conformation was observed for p47phox^{AIR} compared to p47phox$^{SH3A\text{-}B}$ (Fig. S9D-F, Table S2), as shown by Yuzawa et al. [16]. Possible alterations of p47phox^{AIR} upon addition of p22phox-derived peptides were not previously investigated; however, our data did not indicate any differences between p47phox^{AIR} with and without p22phox$^{149\text{-}168}$ (Fig. S9D-F, Table S2). In contrast to the p22phox peptides, no significant conformational changes in p47phox$^{SH3A\text{-}B}$ were observed with any of the eight fragments at either 2 or 4 mM (Fig. 3G-H). One fragment with high solubility (fragment hit **8**), was tested also at a 10 mM concentration, showing no difference between any of the concentrations (data not shown). These SAXS data indicate that the fragments bind to an extended conformation of p47phox$^{SH3A\text{-}B}$.

SPR binding level as a measure to elucidate binding stoichiometry. The NMR experiments of p47phox$^{SH3A\text{-}B}$ with the fragment hits **1** and **2** show an influence of fragments binding on chemical shifts of Trp residues in both the SH3A and SH3B domains of p47phox. The SAXS data show that all fragments bind to an extended conformation of p47phox$^{SH3A\text{-}B}$, and not a compact conformation as induced upon p22phox binding. This means that the SH3A and SH3B domains of p47phox$^{SH3A\text{-}B}$ are not close enough in space to form a joint extended binding pocket accommodating fragment hits **1** and **2**, which would explain the chemical shift changes of the Trp residues in both SH3 domains of p47phox$^{SH3A\text{-}B}$. An alternative explanation could be that two binding pockets for fragments exist in p47phox$^{SH3A\text{-}B}$, one in the SH3A

domain and one in the SH3B domain. To investigate this, the eight fragments were injected in a one-step concentration gradient [37, 38] at 1 mM over immobilized p47phox^{SH3A-B} (2745 RU) allowing a direct comparison of the molecular weight (MW) normalized response levels of the eight fragments (Fig. 3I). The response levels of **1** and **2** were approximately 2-fold higher compared to **3**-**8**, clearly indicating that **1** and **2** have two binding-sites at p47phox^{SH3A-B}, while **3**-**8** likely have one, in support of the NMR results.

Competition between p22phox and fragments for binding to p47phox^{SH3A-B}. The ability of **1**-**8** to compete with p22phox for binding to p47phox^{SH3A-B} was investigated in SPR competition assays. First, this was done in a two-component injection experiment where p22phox$^{149-168}$ (10 μM) was injected over immobilized p47phox^{SH3A-B} followed by a continuous gradient injection of fragments (up to 1 mM), while the p22phox$^{149-168}$ concentration was kept constant (Fig. 3J). These experiments were performed directly after the injections shown in Fig. 3I, whereby the normalized binding levels in Fig. 3I and Fig. 3J can be directly compared. The response levels for all eight fragments binding to p47phox^{SH3A-B} was significantly reduced when they were injected with p22phox$^{149-168}$ (Fig. 3J), which shows that when p47phox^{SH3A-B} is already binding p22phox$^{149-168}$, the ability of the fragments to bind p47phox^{SH3A-B} is reduced. The second competition assay was performed oppositely by injecting the fragments constantly at 1 mM over immobilized p47phox^{SH3A-B} and subsequently, whilst continuously injecting these, adding p22phox$^{149-168}$ (10 μM) by one-step gradient injection (Fig. S10). Comparing the experimental response levels with the expected theoretical response, based on calculated response if both fragment and p22phox$^{149-168}$ are able to bind simultaneously to p47phox^{SH3A-B}, revealed that only fragments **1** and **2** were able to reduce the total binding level by more than 5% and thus compete with p22phox$^{149-168}$ for binding to p47phox^{SH3A-B} (Table S4). The results from the two SPR competition assays illustrate that the ability for competition is influenced by the order of injection of the competing components. When injecting p22phox$^{149-168}$ before the fragments were injected, the p47phox^{SH3A-B} exists in a more compact peptide-bound conformation and in this case all fragment hits poorly bind p47phox^{SH3A-B}. In the experiments where the fragments were continuously injected before p22phox$^{149-168}$, we presume that p47phox^{SH3A-B} exist in a more elongated conformation, and in this case fragments **1** and **2** were able to reduce p22phox$^{149-168}$ binding. Fragments **3**-**8** were not able to reduce p22phox binding to p47phox, suggesting that p22phox and fragments **3**-**8** can bind p47phox simultaneously. Thus, the SPR and FP competition experiments demonstrated that only fragments **1** and **2** could inhibit p47phox^{SH3A-B} binding to p22phox.

Structure Activity Relationship studies of fragments 1 and 2. Fragment hits **1** and **2**, which share the quinoline scaffold (Fig. 2J), were selected for SAR studies (Fig. 4A). These fragments were the only hits originating as common FP and TSA screen hits and were validated in all SPR assays. Additionally, **1** and **2** showed chemical shift changes of all five Trp indole NHs of p47phox^{SH3A-B}. These NMR data together with the SAXS and SPR data, suggested binding to two sites at the extended conformation of p47phox^{SH3A-B}, one in the SH3A and one in the SH3B domain. Initially, 21 analogues (**9**-**29**) of fragment **2** and 41 analogues (**30**-**70**) of fragment **1** were purchased or synthesized (Scheme S1) and tested by FP and SPR (See detailed SAR discussion and K_i and K_D values from FP and SPR in Table S5-6). This SAR study explored several substitutions on the quinoline ring, in order to obtain information for further directions of optimization. Several analogs showed improved affinities relative to parent fragment hit **1** and **2**, however, to a rather

modest extent with K_i values decreased 2-3-fold for compound **13, 15, 20, 28, 54, 56, 63, 64 and 67** relative to the parent fragment hits (Table S5-6) Fig. 4 shows representative FP and SPR data for analogs with reduced, similar or improved activity). For example compound **64**, is a structural merge of **1** and **2** as it contains both the amino and piperazine groups found important for affinity, with a K_D of 78 μM to p47phox^{SH3A-B} measured by SPR and a K_i of 196 μM measured by FP. Also, adding a bromine at the 6-position of the quinolone scaffold as in **20** led to a 3-fold affinity increase as measured by FP (Table S5-6). Still, it seemed that to obtain more dramatic improvements in p22phox inhibitory activity and binding affinity, more unconventional means were required. Hence, considering that our SPR and NMR data (Fig. 3 and S8) suggest that **1** and **2** bind to both SH3 domains of p47phox, we envisioned that connecting these fragments by a linker affording a homodimeric compound would lead to more significant affinity improvements, as has been reported for other protein targets [39-41]. Based on our SAR study, the 4-, 6-, 7-positions could provide suitable attachment points for linkers. Thus, the three dimeric compounds **71-73** were designed and synthesized (Scheme 1). As anticipated, the three dimers gave a 13–30-fold improved affinity by FP compared to the monomeric parent fragment hits **1** and **2** (Table S6). Among the three dimeric compounds, **71** was the most potent dimer with a K_i of 20 μM in FP, which is similar to the p22phox$^{151-162}$ peptide (K_i = 17 μM at 2% DMSO), and with confirmed binding in SPR (K_D = 50 μM) (Fig. 4I-J). As a control experiment, we tested **71-73** by FP in the presence of 0.01% Triton-X to probe for potential aggregation artifacts. All compounds showed same affinities as without the presence of Triton-X within the experimental error (Fig. S11).

Discussion

The assembly of the cytosolic subunits with the membrane bound NOX2 subunits is a critical step for NOX2 activation in relation to cancers, inflammation and CNS diseases, as explored using knock-out animal models and pharmacological studies [5, 7, 19]. A key event in NOX2 activation is the docking of p22phox to p47phox (Fig. 5A). Thus inhibition of the p47phox-p22phox interaction is a potential strategy for therapeutic intervention against oxidative stress.

To date, only the seleno-organic ROS scavenging compound ebselen has been shown to inhibit NOX2 activity by binding to p47phox, thereby preventing its interaction with p22phox [19]. Here, we show that ebselen covalently reacts with Cys^{196} of p47phox, leading to destabilization and aggregation of the protein. This dramatic effect can be explained by Cys^{196} being localized directly adjacent to residues Trp^{193}, Trp^{204}, Phe^{195} and Val^{186}, reported to form the hydrophobic binding pocket for p22phox in the p47phox SH3A domain [15]. Although this mechanism of action of ebselen prevents p47phox from binding to p22phox, resulting in reduced NOX2 activity as described [19], such a mechanism does not seem promising for further drug development, nor a useful property for a chemical probe, as it likely comes with unspecific and potential toxic effects. Indeed, ebselen has been found active against several proteins, and is thus a non-selective compound [42-46].

To identify fragments binding to p47phox, which could be used as scaffolds for developing reversible and druglike inhibitors of the p47phox-p22phox interaction, we performed a fragment screen against p47phox^{SH3A-B} using a competitive FP assay and TSA as primary screening methods and SPR as the main validation technique. To select the most promising hits for SAR analysis, direct binding and functional competitive activity with p22phox were verified using a wide range of assay setups. This resulted in eight fragment hits (**1-8**) being identified and prioritized. These fragments exhibited differences in the binding modes as revealed from the binding stoichiometry in SPR and structural

validation studies based on NMR. Interestingly, none of the fragments showed in SAXS studies any sign of being able to induce the compact conformation of p47phox^{SH3A-B}, as observed when in complex with p22phox. Instead a more extended conformation was retained.

The quinolone fragment hits **1** and **2** had interesting properties. They were the only common hits across all assays, and binding as well as structural data suggested that they interact with two sites on p47phox^{SH3A-B}, presumably at the SH3A and SH3B domain, respectively (Fig. 5B). The competition assays also showed that these two fragments were the only ones able to reduce the ability for p22phox to bind p47phox. This we propose could be either due to the fragments sterically preventing p22phox$^{149-168}$ binding or because the fragments stabilize the extended conformation of p47phox^{SH3A-B} and prevent the formation of the compact conformation required for creating the binding pocket to p22phox$^{149-168}$. The binding stoichiometry and structural data of fragments **4**, **5** and **7** revealed binding to only the SH3A domain of p47phox^{SH3A-B} and no inhibition of binding between p22phox$^{149-168}$ and p47phox (Fig. 5C). Thus, these fragments were considered less interesting for further SAR studies. For fragments **3**, **6**, and **8**, it was not clear from the NMR titration experiments if they were binding to one or two sites at p47phox, but from the SPR binding stoichiometry data, they appeared to only bind one site, similarly to fragments **4**, **5** and **7**.

The most promising fragment hits, **1** and **2**, were selected for SAR analysis resulting in design and synthesis of 65 analogs. Several smaller modifications gave affinity improvements of 2–3-fold compared to parent fragment hits. However, the biggest improvement in affinity was obtained by connecting fragments **1** and **2** by a PEG-based linker, affording the three homodimeric compounds **71**-**73** with 13–30-fold higher affinities than **1** and **2,** and the best dimer (**71**) being equipotent to the p22phox$^{151-162}$ peptide (K_i = 20 μM)**.** This dimeric design was incited by our SPR, SAXS, and NMR data suggesting that **1** and **2** bind to both SH3 domains of p47phox, and the improved affinity seen for the dimeric compounds seems to support the proposed binding mode of the fragments (Fig. 5B). Interestingly, the 2-aminoquinoline ring has previously been reported as a useful scaffold for the development of small-molecule ligands for SH3 domains [47]. NMR binding studies of 2-aminoquinoline with the mouse Tec Kinase SH3 indicated that the two residues Trp^{215} and Asp^{196} in the Tec kinase SH3 sequence, which form part of the proline-rich peptide binding site in this protein, are important for binding to occur. In sequence alignments of the mouse Tec Kinase SH3 domain with the two SH3 domains of p47phox (Fig. S12), the mouse Tec Kinase domain residue Trp^{215} is conserved for both SH3A (equal to Trp^{193}) and SH3B (equal to Trp^{263}), while Asp^{196} is conservatively exchanged to a glutamic acid in p47phox SH3A (Glu^{174}) and SH3B (Glu^{254}) [13, 47]. Combined with our data, this homology further supports the model of **1** and **2** binding to the extended conformation of p47phox^{SH3A-B}, at binding sites composed of key amino acids at both SH3A (Glu^{174}, Trp^{193}) and SH3B (Glu^{254}, Trp^{263}).

By screening 2,500 fragments followed by thorough validation tests, characterization of the binding mode and SAR studies of the most promising hits, we have developed the first non-peptide reversible inhibitors of the p47phox-p22phox protein-protein interaction. The best compounds are dimeric with affinities similar to the shorter p22phox-derived peptide p22phox$^{151-162}$. Although further optimization is needed to reach affinities relevant for more advanced biological studies, our SAR study and proposed binding model based on biophysical and structural data provide encouraging results and guidance for future directions. Hopefully these data can facilitate development of suitable chemical probes for studying the therapeutic relevance of inhibiting NADPH oxidase assembly and activity.

Acknowledgments

This research was supported by the Lundbeck Foundation (Grant R190-2014-3710 for A.B.); the Ragna Rask Basic Research Foundation (for S.S); the China Scholarship Council (File no. 2017062200 for J.Z.); the A.P. Møller Foundation for the Advancement of Medical Science (Grant 14-28 for A.B.); the Hørslev Foundation (Grant 203866-MIA for A.B.); the Augustinus Foundation (Grant 14-1571 for A.B.); the Novo Nordisk Foundation SYNERGY project (Grant NNF15OC0016670 for S.B.); the Lundbeck Foundation Initiative BRAINSTRUC (Grant 2015-2666 for A.E.L), and the EU Horizon 2020 Marie Skołdowska-Curie grant (Grant 675555 (AEGIS) for C.S. and M.S.). We would also like to thank Dr. Kenji Ogura for kindly providing the chemical shifts of the solution NMR structure of p47phox^{SH3A-B} in complex with p22phox previously published in Ogura et al., JBC 2006 [15]. We acknowledge access to NMR measurements at the Bavarian NMR Center and the NMR Center DTU, supported by the Villum Foundation.

References

1. Diebold, B.A., et al., *NOX2 As a Target for Drug Development: Indications, Possible Complications, and Progress.* Antioxid Redox Signal, 2015. **23**(5): p. 375-405.

2. Sukumar, P., et al., *Nox2 NADPH oxidase has a critical role in insulin resistance-related endothelial cell dysfunction.* Diabetes, 2013. **62**(6): p. 2130-4.

3. Block, K. and Y. Gorin, *Aiding and abetting roles of NOX oxidases in cellular transformation.* Nat Rev Cancer, 2012. **12**(9): p. 627-37.

4. Bedard, K. and K.H. Krause, *The NOX family of ROS-generating NADPH oxidases: physiology and pathophysiology.* Physiol Rev, 2007. **87**(1): p. 245-313.

5. Drummond, G.R., et al., *Combating oxidative stress in vascular disease: NADPH oxidases as therapeutic targets.* Nat Rev Drug Discov, 2011. **10**(6): p. 453-71.

6. Tang, X.N., et al., *Significance of marrow-derived nicotinamide adenine dinucleotide phosphate oxidase in experimental ischemic stroke.* Ann Neurol, 2011. **70**(4): p. 606-15.

7. Bach, A., *Targeting Oxidative Stress in Stroke.* , in *Chapter 8 Neuroprotective Therapy for Stroke and Ischemic Disease*, P. Lapchak and J. Zhang, Editors. 2017, Springer Series in Translational Stroke Research.

8. Groemping, Y. and K. Rittinger, *Activation and assembly of the NADPH oxidase: a structural perspective.* Biochem J, 2005. **386**(Pt 3): p. 401-16.

9. El-Benna, J., et al., *p47phox, the phagocyte NADPH oxidase/NOX2 organizer: structure, phosphorylation and implication in diseases.* Exp Mol Med, 2009. **41**(4): p. 217-25.

10. Faust, L.R., et al., *The phosphorylation targets of p47phox, a subunit of the respiratory burst oxidase. Functions of the individual target serines as evaluated by site-directed mutagenesis.* J Clin Invest, 1995. **96**(3): p. 1499-505.

11. Inanami, O., et al., *Activation of the leukocyte NADPH oxidase by phorbol ester requires the phosphorylation of p47PHOX on serine 303 or 304.* J Biol Chem, 1998. **273**(16): p. 9539-43.

12. Johnson, J.L., et al., *Activation of p47(PHOX), a cytosolic subunit of the leukocyte NADPH oxidase. Phosphorylation of ser-359 or ser-370 precedes phosphorylation at other sites and is required for activity.* J Biol Chem, 1998. **273**(52): p. 35147-52.

13. Groemping, Y., et al., *Molecular basis of phosphorylation-induced activation of the NADPH oxidase.* Cell, 2003. **113**(3): p. 343-55.

14. Sumimoto, H., et al., *Assembly and activation of the phagocyte NADPH oxidase. Specific interaction of the N-terminal Src homology 3 domain of p47phox with p22phox is required for activation of the NADPH oxidase.* J Biol Chem, 1996. **271**(36): p. 22152-8.

15. Ogura, K., et al., *NMR solution structure of the tandem Src homology 3 domains of p47phox complexed with a p22phox-derived proline-rich peptide.* J Biol Chem, 2006. **281**(6): p. 3660-8.

16. Yuzawa, S., et al., *Solution structure of the tandem Src homology 3 domains of p47phox in an autoinhibited form.* J Biol Chem, 2004. **279**(28): p. 29752-60.

17. Yuzawa, S., et al., *Crystallization and preliminary crystallographic analysis of the autoinhibited form of the tandem SH3 domain of p47(phox).* Acta Crystallogr D Biol Crystallogr, 2003. **59**(Pt 8): p. 1479-80.

18. Yuzawa, S., et al., *A molecular mechanism for autoinhibition of the tandem SH3 domains of p47phox, the regulatory subunit of the phagocyte NADPH oxidase.* Genes Cells, 2004. **9**(5): p. 443-56.

19. Smith, S.M., et al., *Ebselen and congeners inhibit NADPH oxidase 2-dependent superoxide generation by interrupting the binding of regulatory subunits.* Chem Biol, 2012. **19**(6): p. 752-63.

20. Haenen, G.R., et al., *Mechanism of the reaction of ebselen with endogenous thiols: dihydrolipoate is a better cofactor than glutathione in the peroxidase activity of ebselen.* Mol Pharmacol, 1990. **37**(3): p. 412-22.

21. Sakurai, T., et al., *Ebselen, a seleno-organic antioxidant, as an electrophile.* Chem Res Toxicol, 2006. **19**(9): p. 1196-204.

22. Macias Perez, M.E., et al., *Aromatic Regions Govern the Recognition of NADPH Oxidase Inhibitors as Diapocynin and its Analogues.* Arch Pharm (Weinheim), 2017. **350**(10).

23. Macias-Perez, M.E., et al., *Ethers and esters derived from apocynin avoid the interaction between p47phox and p22phox subunits of NADPH oxidase: evaluation in vitro and in silico.* Biosci Rep, 2013. **33**(4).

24. Ago, T., et al., *Mechanism for phosphorylation-induced activation of the phagocyte NADPH oxidase protein p47(phox). Triple replacement of serines 303, 304, and 328 with aspartates disrupts the SH3 domain-mediated intramolecular interaction in p47(phox), thereby activating the oxidase.* J Biol Chem, 1999. **274**(47): p. 33644-53.

25. Carr, R.A., et al., *Fragment-based lead discovery: leads by design.* Drug Discov Today, 2005. **10**(14): p. 987-92.

26. Feng, B.Y. and B.K. Shoichet, *A detergent-based assay for the detection of promiscuous inhibitors.* Nat Protoc, 2006. **1**(2): p. 550-3.

27. McGovern, S.L., et al., *A specific mechanism of nonspecific inhibition.* J Med Chem, 2003. **46**(20): p. 4265-72.

28. Ryan, A.J., et al., *Effect of detergent on "promiscuous" inhibitors.* J Med Chem, 2003. **46**(16): p. 3448-51.

29. Owicki, J.C., *Fluorescence polarization and anisotropy in high throughput screening: perspectives and primer.* J Biomol Screen, 2000. **5**(5): p. 297-306.

30. Pope, A.J., U.M. Haupts, and K.J. Moore, *Homogeneous fluorescence readouts for miniaturized high-throughput screening: theory and practice.* Drug Discov Today, 1999. **4**(8): p. 350-362.

31. Turconi, S., et al., *Real experiences of uHTS: a prototypic 1536-well fluorescence anisotropy-based uHTS screen and application of well-level quality control procedures.* J Biomol Screen, 2001. **6**(5): p. 275-90.

32. Turek-Etienne, T.C., et al., *Evaluation of fluorescent compound interference in 4 fluorescence polarization assays: 2 kinases, 1 protease, and 1 phosphatase.* J Biomol Screen, 2003. **8**(2): p. 176-84.

33. Vedvik, K.L., et al., *Overcoming compound interference in fluorescence polarization-based kinase assays using far-red tracers.* Assay Drug Dev Technol, 2004. **2**(2): p. 193-203.

34. Giannetti, A.M., et al., *Chapter 2 Getting the Most Value from Your Screens: Advances in Hardware, Software, and Methodologies to Enhance Surface Plasmon Resonance Based Fragment Screening and Hit-to-Lead Support.* Fragment-Based Drug Discovery, 2015: p. 19-48.

35. Lagorce, D., et al., *FAF-Drugs4: free ADME-tox filtering computations for chemical biology and early stages drug discovery.* Bioinformatics, 2017. **33**(22): p. 3658-3660.

36. Irwin, J.J., et al., *An Aggregation Advisor for Ligand Discovery.* J Med Chem, 2015. **58**(17): p. 7076-87.

37. Quinn, J.G., *Evaluation of Taylor dispersion injections: determining kinetic/affinity interaction constants and diffusion coefficients in label-free biosensing.* Anal Biochem, 2012. **421**(2): p. 401-10.

38. Quinn, J.G., *Modeling Taylor dispersion injections: determination of kinetic/affinity interaction constants and diffusion coefficients in label-free biosensing.* Anal Biochem, 2012. **421**(2): p. 391-400.

39. Pulido, D., et al., *Design of a True Bivalent Ligand with Picomolar Binding Affinity for a G Protein-Coupled Receptor Homodimer.* J Med Chem, 2018. **61**(20): p. 9335-9346.

40. Bach, A., et al., *Design and synthesis of highly potent and plasma-stable dimeric inhibitors of the PSD-95-NMDA receptor interaction.* Angew Chem Int Ed Engl, 2009. **48**(51): p. 9685-9.

41. Krishnamurthy, V.M., et al., *Dependence of effective molarity on linker length for an intramolecular protein-ligand system.* J Am Chem Soc, 2007. **129**(5): p. 1312-20.

42. Baek, J.M., et al., *Ebselen Is a Potential Anti-Osteoporosis Agent by Suppressing Receptor Activator of Nuclear Factor Kappa-B Ligand-Induced Osteoclast Differentiation In vitro and Lipopolysaccharide-Induced Inflammatory Bone Destruction In vivo.* Int J Biol Sci, 2016. **12**(5): p. 478-88.

43. Bender, K.O., et al., *A small-molecule antivirulence agent for treating Clostridium difficile infection.* Sci Transl Med, 2015. **7**(306): p. 306ra148.

44. Singh, N., et al., *Effect of the Putative Lithium Mimetic Ebselen on Brain Myo-Inositol, Sleep, and Emotional Processing in Humans.* Neuropsychopharmacology, 2016. **41**(7): p. 1768-78.

45. Thangamani, S., et al., *Ebselen exerts antifungal activity by regulating glutathione (GSH) and reactive oxygen species (ROS) production in fungal cells.* Biochim Biophys Acta Gen Subj, 2017. **1861**(1 Pt A): p. 3002-3010.

46. Beilhartz, G.L., et al., *Comment on "A small-molecule antivirulence agent for treating Clostridium difficile infection".* Sci Transl Med, 2016. **8**(370): p. 370tc2.

47. Inglis, S.R., et al., *Identification and specificity studies of small-molecule ligands for SH3 protein domains.* J Med Chem, 2004. **47**(22): p. 5405-17.

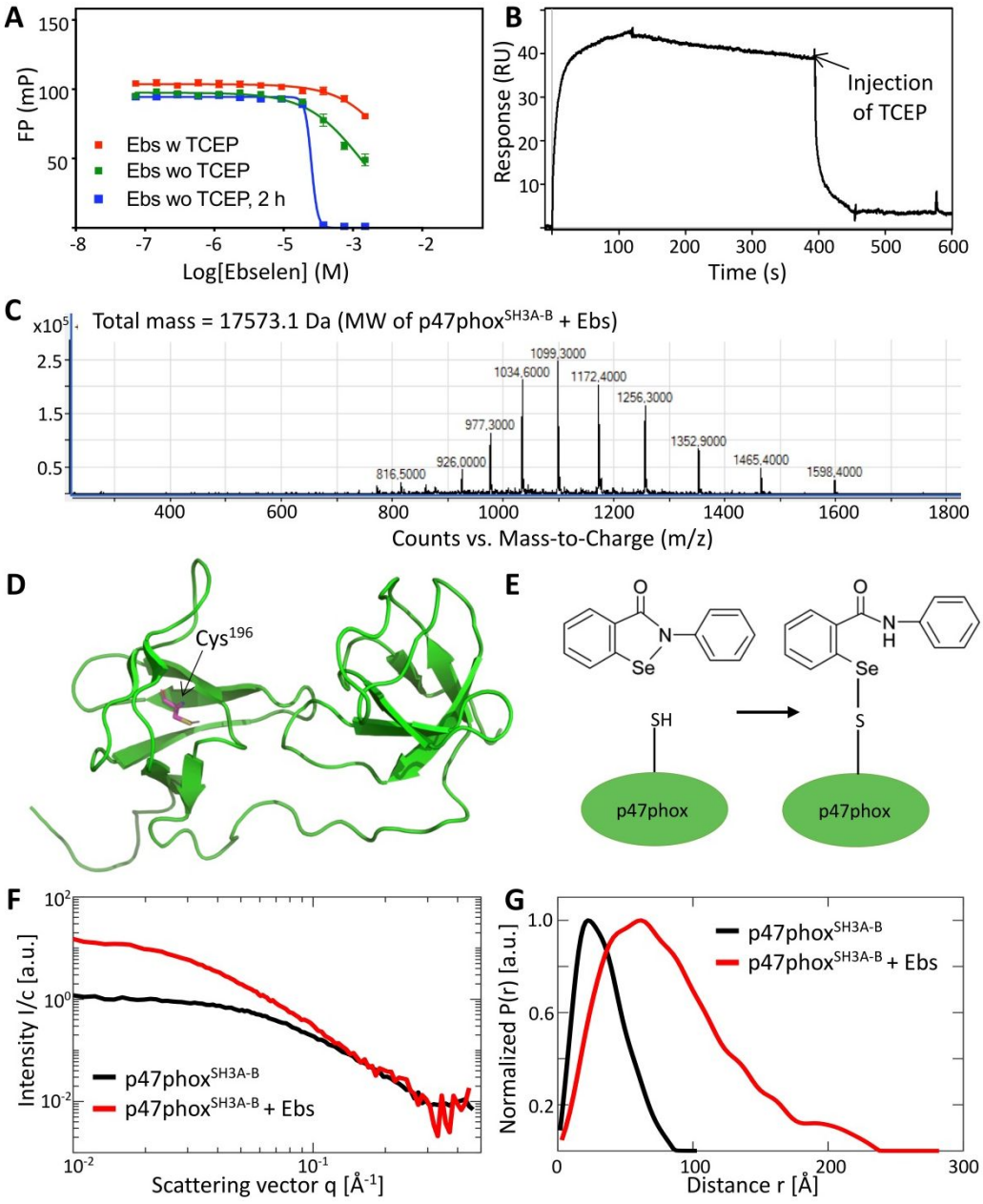

Figure 1. Interaction of p47phox^{SH3A-B} with ebselen. A) FP competition binding assay for ebselen competing with the fluorescent probe Cy5-p22phox$^{149-162}$ for binding to p47phox^{SH3A-B} with (blue) and without (red) TCEP in the buffer. Both experiments were carried out in duplicate, each with n=3. B) SPR sensorgram of ebselen (12.5 µM) injected over 4684 RU immobilized p47phox^{SH3A-B} on a biosensor chip followed by abrogation of the complex by injection of buffer supplemented with 2 mM TCEP. C) LCMS data of 0.2 mg/mL p47phox^{SH3A-B} with 200 µM ebselen showing a total mass of 17573.1 ± 0.5 Da. D) The solution NMR structure of p47phox^{SH3A-B} when in complex with p22phox$^{149-168}$ (PDB ID: 1WLP) where the single cysteine residue (Cys^{196}) situated in the SH3A domain is highlighted (purple) (the p22phox peptide is removed here). E) Proposed binding mode of ebselen to p47phox^{SH3A-B}, where ebselen forms a selenylsulphide bond with the Cys^{196} of p47phox^{SH3A-B}, thus forming a stable complex. F) SAXS data for p47phox^{SH3A-B} (black) and p47phox^{SH3A-B} in the presence of ebselen (red) plotted as concentration-normalized scattering intensity I(q)/c in arbitrary units vs. q and G) the corresponding pair-distance distribution function P(r).

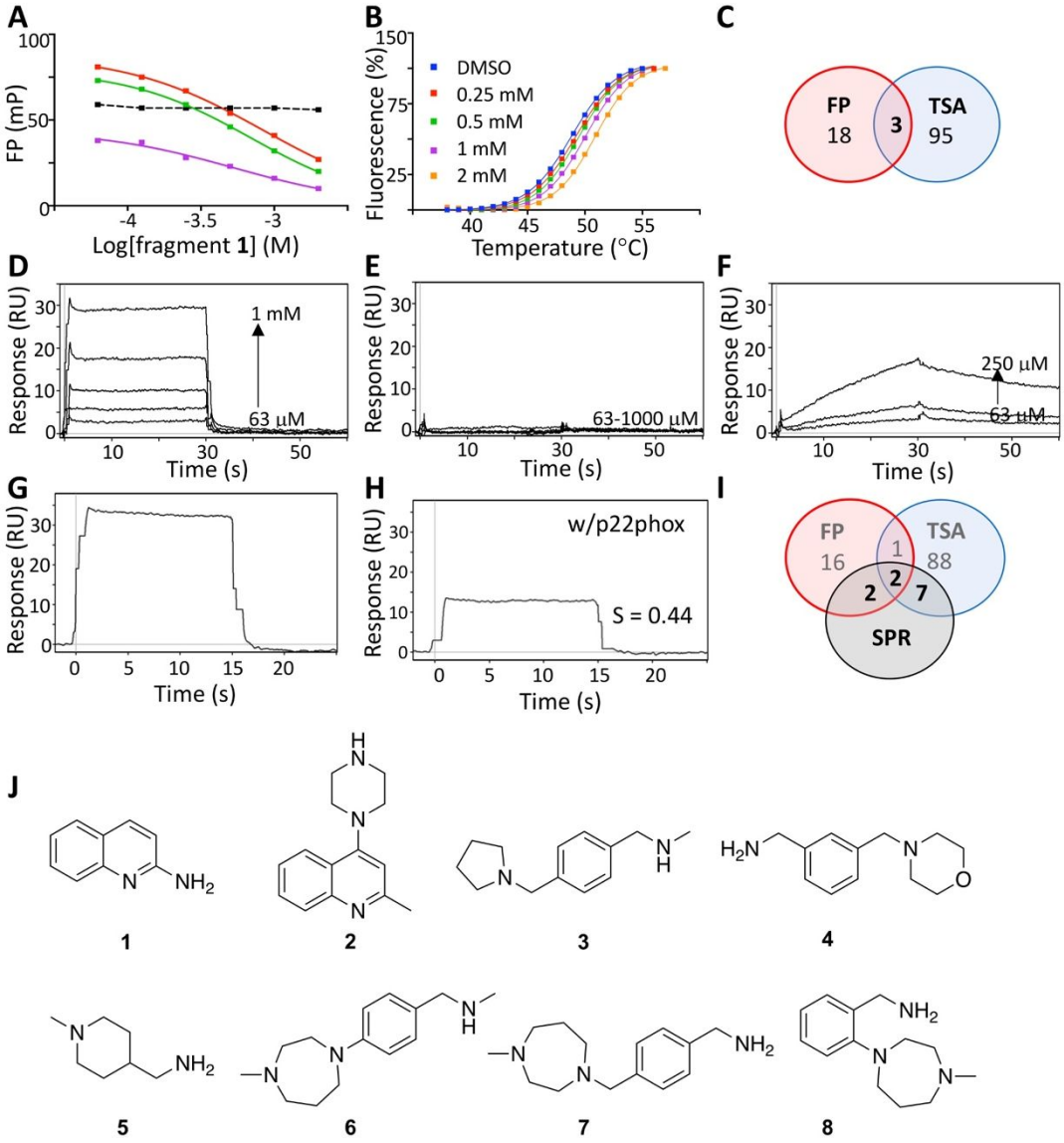

Figure 2. Examples from fragment screening and initial hit validation. A) FP competition binding assay for fragment hit **1** competing with the fluorescent probe Cy5-p22phox$^{149\text{-}162}$ (red) and TAMRA- p22phox$^{151\text{-}162}$ (purple) for binding to p47phox$^{SH3A\text{-}B}$. As control, the assay was performed in presence of 0.01% detergent (Triton-X) to exclude aggregation-based promiscuous inhibitors (green) and without protein (black). B) Unfolding transition of p47phox$^{SH3A\text{-}B}$ with increasing temperature in the presence of fragment **1** measured by TSA. C) The numbers of validated screen hits from FP, TSA assay and both assays presented in a Venn diagram. D-F) The FP and TSA validated screen hits were injected over immobilized p47phox$^{SH3A\text{-}B}$ on a biosensor chip to validate their binding behavior by SPR. Fragments showing a concentration dependent binding response and a fragment-like binding kinetic (as for fragment **1** example in D) were confirmed as hits. Fragments that showed no binding up to a concentration of 1 mM (as example in E) or a non-fragment-like binding behavior (as example in F) were not regarded as true hits. G, H) The confirmed hits in SPR binding assays were investigated in an SPR inhibition assay for binding to the relevant site at p47phox$^{SH3A\text{-}B}$. One mM fragment was injected over immobilized p47phox$^{SH3A\text{-}B}$ (3358 RU) in the absence G) and in the presence H) of 10 µM p22phox$^{149\text{-}168}$ in the running buffer. All SPR sensorgrams are blank injection and reference surface subtracted. An activated and inactivated surface was used as a reference. I) The numbers of final validated screen hits from FP, TSA and SPR are presented in a venn-diagram. J) The chemical structures of the final eight fragments selected for further investigation.

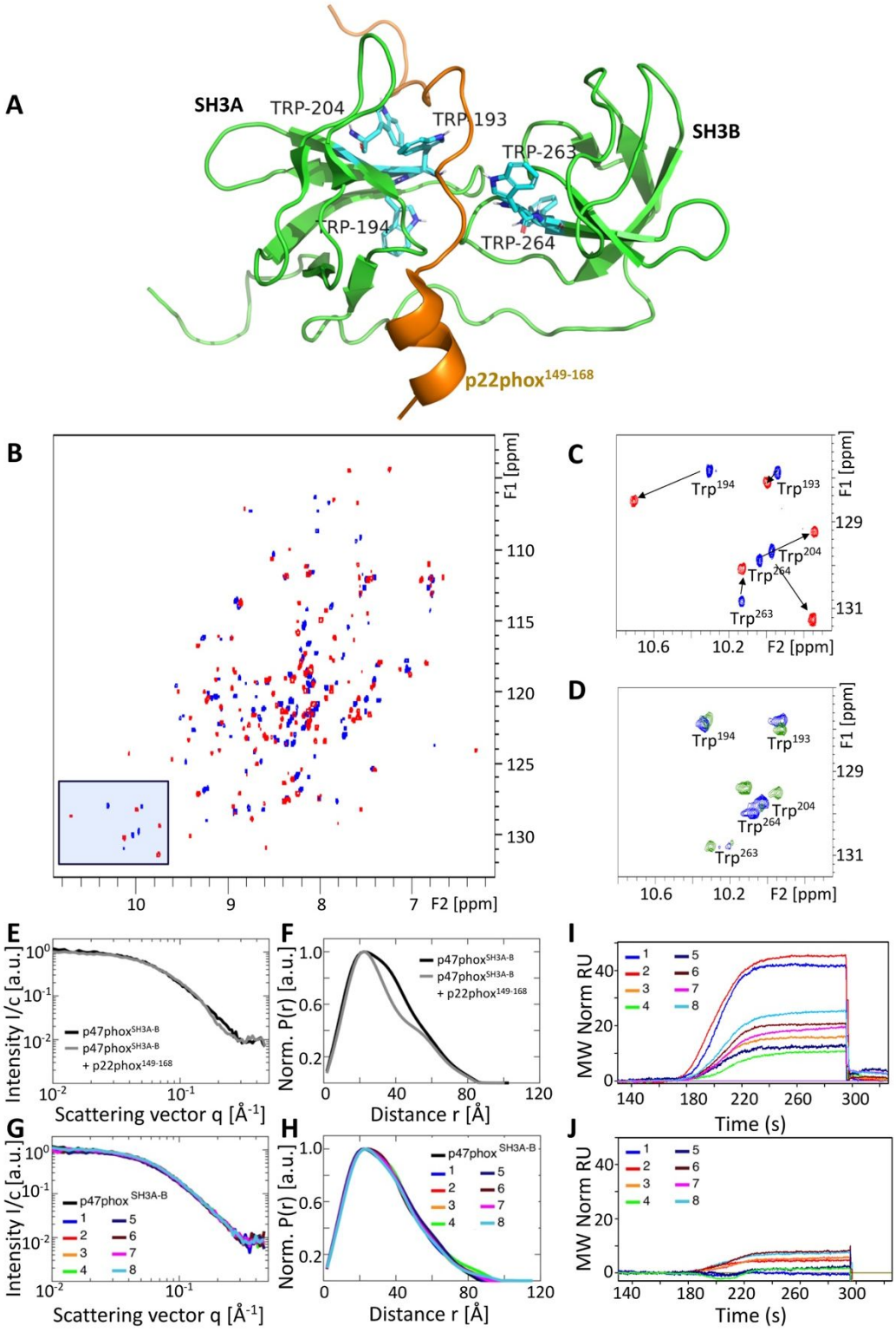

Figure 3. Validation of fragment hits by NMR, SAXS and SPR binding stoichiometry. A) The solution NMR structure of p47phox^{SH3A-B} (green) in complex with p22phox$^{149-168}$ (orange) (PDB ID: 1WLP) where the five Trp indole NH groups of p47phox^{SH3A-B} situated in the binding pocket are highlighted. B) ^{1}H-^{15}N HSQC spectra of p47phox^{SH3A-B} free (blue) and in the presence of 4-fold molar excess of p22phox$^{149-168}$ (red). C) Expanded region with indole NH

signals of the five tryptophan residues in p47phox^{SH3A-B} free (blue) and bound to p22phox$^{149-168}$ (red). D) The same expanded tryptophan indole NH region of p47phox^{SH3A-B} free (blue) superimposed with p47phox^{SH3A-B} in the presence of fragment hit **1** (1:20) (green), both samples supplemented with 4% DMSO. E) SAXS data for p47phox^{SH3A-B} (black) and p47phox in the presence of p22phox$^{149-168}$ (grey) plotted as concentration-normalized scattering intensity I(q)/c in arbitrary units vs. q and F) the corresponding pair-distance distribution function P(r). G) SAXS data for p47phox^{SH3A-B} (black) and p47phox^{SH3A-B} in the presence of fragments plotted as concentration-normalized scattering intensity I(q)/c in arbitrary units vs. q and H) the corresponding pair-distance distribution function P(r). I) The 8 final fragment hits were injected by a one-step gradient injection over immobilized p47phox^{SH3A-B} (2745 RU) to distinguish the differences in MW normalized response maximum binding level. J) SPR inhibition assay where p22phox$^{149-168}$ was injected constantly at 10 μM while injecting a one-step gradient of 1 mM of the fragments over 2745 RU immobilized p47phox^{SH3A-B}.

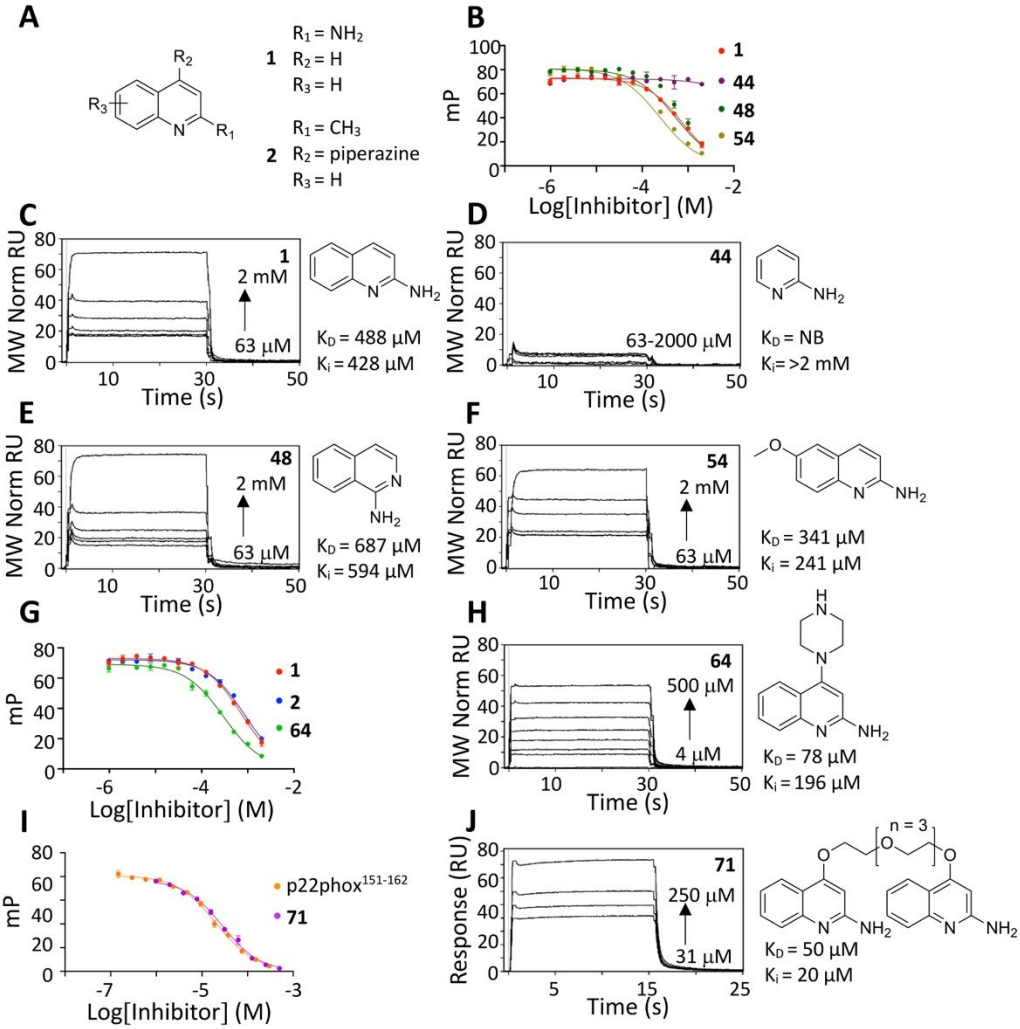

Figure 4. SAR analysis. A) Markush structure of fragment hit **1** and **2**, which structurally share the quinoline scaffold. B) FP competition binding assay for fragment hit **1, 44, 48 and 54** competing with the fluorescent probe Cy5-p22phox$^{149\text{-}162}$ for binding to p47phox$^{SH3A\text{-}B}$. C-F) The fragment analogs **44, 48 and 55** tested for binding to p47phox$^{SH3A\text{-}B}$ compared to their parental fragment **1** by SPR. SPR sensorgrams of fragment hit **1** (C), analog **44** (D), analog **48** (E)**, and analog 55** (F) injected over immobilized p47phox$^{SH3A\text{-}B}$ (5873 RU) on a biosensor chip. The SPR sensorgrams have MW normalized RU. D) Fragment analog **44** did not bind to p47phox$^{SH3A\text{-}B}$. E) Fragment analog **48** binds to p47phox$^{SH3A\text{-}B}$, but with a slightly reduced affinity compared to the fragment hit **1.** F) Fragment analog 55 binds to p47phox$^{SH3A\text{-}B}$ with increased affinity compared to the fragment hit **1.** G) FP competition binding assay for merge analog **64** and parental fragment hit **1** and **2** competing with the fluorescent probe Cy5-p22phox$^{149\text{-}162}$ for binding to p47phox$^{SH3A\text{-}B}$. H) SPR sensorgrams of fragment analog **64** injected over immobilized p47phox$^{SH3A\text{-}B}$ (5873 RU) on a biosensor chip. The SPR sensorgrams have MW normalized RU. I) FP competition binding assay for dimeric compound **71** and parental fragment hit **1** and **2** competing with the fluorescent probe Cy5-p22phox$^{149\text{-}162}$ for binding to p47phox$^{SH3A\text{-}B}$. J) SPR sensorgrams of dimeric compound **71** injected over immobilized p47phox$^{SH3A\text{-}B}$ (5873 RU) on a biosensor chip.

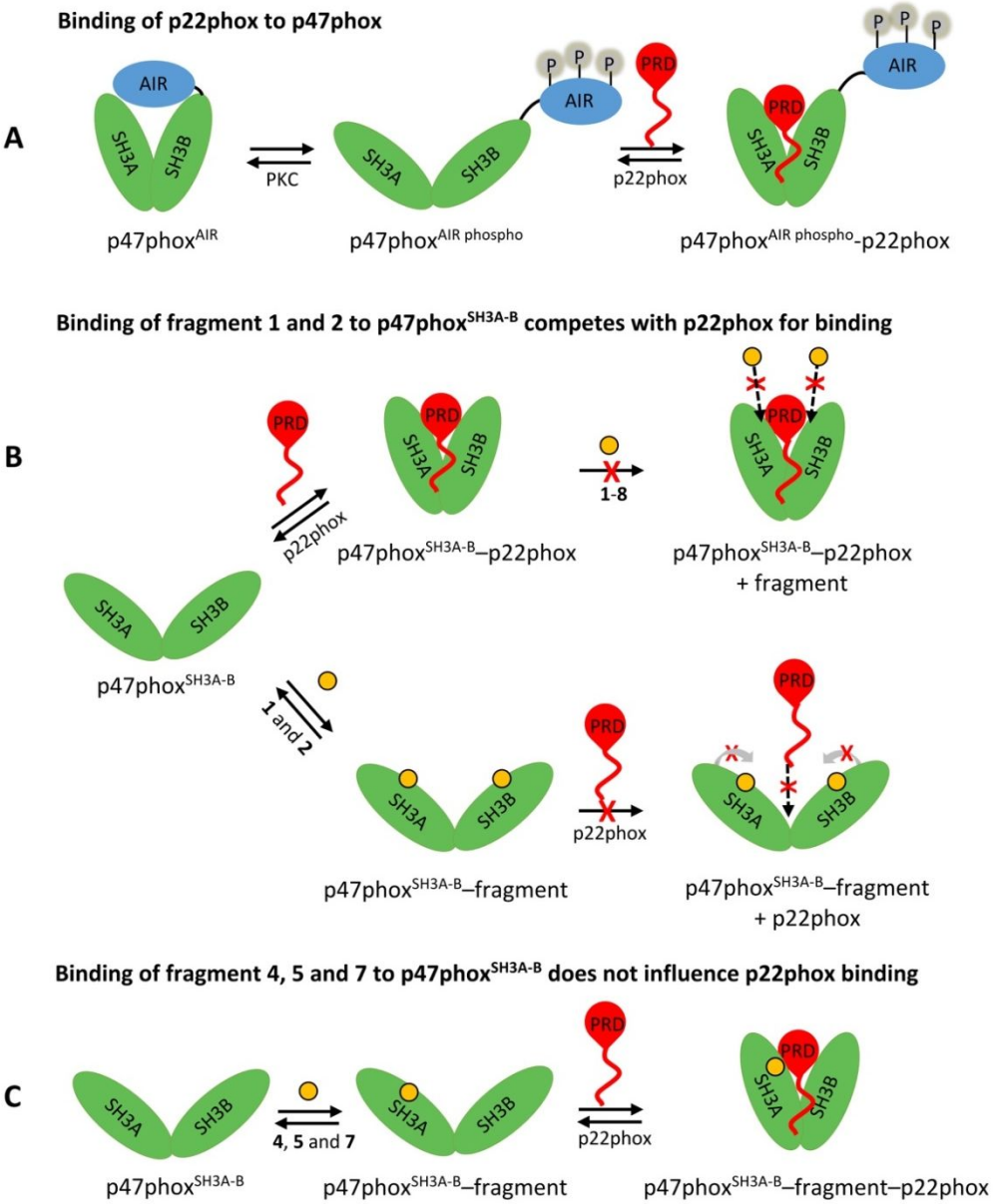

Figure 5. Illustration of fragment hits binding models to p47phox. A) Theoretical model for activation of p47phox^{AIR} by PKC, which phosphorylates seven C-terminal serine residues (of which three are situated in the AIR domain), leading to a conformational change of p47phox where the AIR domain is removed from the tandem SH3 domain and thus opens it for binding to the proline-rich domain (PRD) of p22phox [9]. B) p47phox^{SH3A-B} is a truncated model protein of the activated form, as it includes only the tandem SH3 domains and not the AIR domain. Thus, p47phox^{SH3A-B} does not require phosphorylation to remove the AIR domain for binding to p22phox. Inhibition assays demonstrated that when blocking the tandem SH3 domains of p47phox^{SH3A-B} with the p22phox-derived peptide p22phox$^{149-168}$, which includes the PRD, the fragments ability to bind p47phox^{SH3A-B} was significantly reduced. Fragment hit **1** and **2** were found to bind to two sites of the extended conformation of p47phox^{SH3A-B}, a pocket in SH3A and a pocket in the SH3B domain. From competition assays, the binding of fragment hit **1** and **2** to p47phox^{SH3A-B} reduced p22phox$^{149-168}$ binding. This effect of fragment **1** and **2** could be either due to sterically preventing p22phox$^{149-168}$ binding or because the fragments stabilize the extended conformation of p47phox^{SH3A-B} and prevent the formation of the compact conformation required for creating the binding pocket to p22phox$^{149-168}$. C) Fragment hit **4**, **5** and **7** were found to bind to only the SH3A domain, and competition assays show that these fragments do not influence the binding between p47phox^{SH3A-B} and p22phox$^{149-168}$.

Table 1. Biophysical data of the final 8 validated fragments. ΔT_m was calculated from TSA data, K_i from FP, steady state affinities K_D from SPR sensorgrams in Fig. S6.

Compds	Compd identity	MW	ΔT_m(°C) (0.25/0.5/1/2 mM)	K_i (μM)[a]	K_D (μM)[a]	S[b]
1	2-aminoquinoline	144.2	0.3/0.6/1.2/2.0	428 ± 23	488 ± 130	0.61 ± 0.2
2	2-methyl-4-(piperazin-1-yl) quinoline	227.3	0.7/1.4/2.1/3.6	606 ± 25	412 ± 130	0.48 ± 0.1
3	*N*-methyl-1-(4-(pyrrolidin-1-yl-methyl)phenyl)methanamine	204.3	0.4/0.4/1.7/3.0	No hit	465 ± 160	0.25 ± 0.07
4	(3-(morpholinomethyl) phenyl)methanamine	206.3	1.0/0.9/1.4/2.2	No hit	563 ± 320	0.38 ± 0.2
5	(1-methylpiperidin-4-yl) methanamine	128.2	0.8/0.8/0.9/2.4	No hit	349 ± 29	0.75 ± 0.3
6	*N*-methyl-1-(4-(4-methyl-1,4-diazepan-1-yl) phenyl)methanamine	233.4	0.6/0.8/1.6/2.9	No hit	548 ± 160	0.22 ± 0.05
7	(4-((4-methyl-1,4-diazepan-1-yl)methyl)phenyl)methanamine	233.4	0.5/0.3/1.1/2.0	No hit	418 ± 83	0.36 ± 0.06
8	(2-(4-methyl-1,4-diazepan-1-yl)phenyl)methanamine	219.3	-0.1/0.3/0.9/1.4	No hit	504 ± 110	0.35 ± 0.10

[a] K_i and K_D values are reported as the mean ± SEM ($n \geq 3$); [b] S values are reported as mean ± SEM ($n = 2$)

Scheme 1. Synthesis of dimeric p47phox/p22phox inhibitors compound 71, 72, and 73.

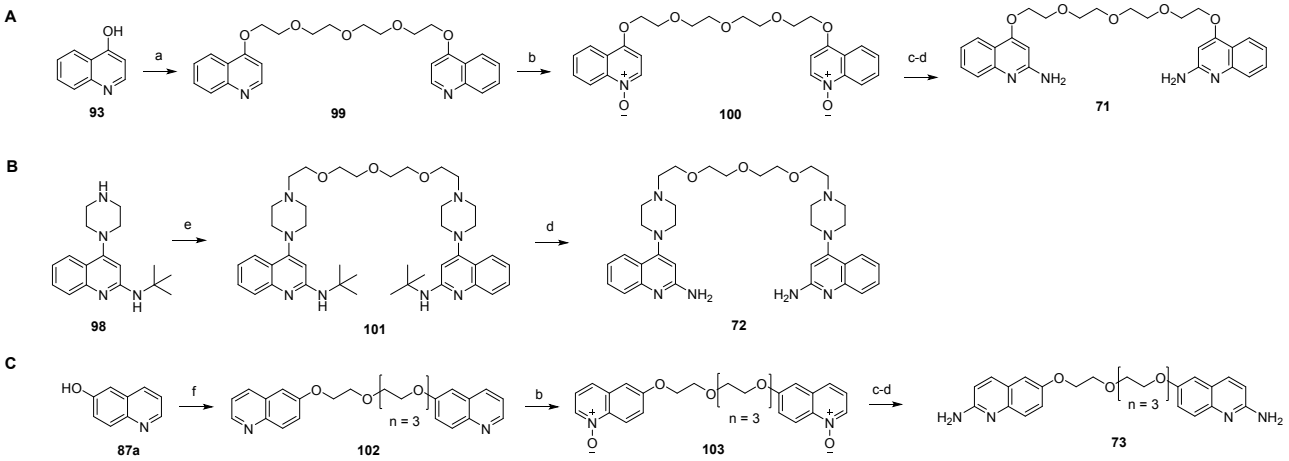

Reagents and conditions: (a) Cs_2CO_3, 1,11-dibromo-3,6,9-trioxaundecane, DMF, 80 °C, 2 h; (b) *m*-CPBA, DCM, 0 °C to rt, overnight; (c) *tert*-butylamine, *p*-toluenesulfonic anhydride, trifluorotoluene, DCM, 0 °C to rt, 30 min; (d) TFA, reflux, 3 h; (e) tetraethylene glycol, K_2CO_3, rt, overnight; (f) tetraethylene glycol, PPh_3, DIAD, THF, rt, 72 h.